

Transient slowing down relaxation dynamics of the supercooled dusty plasma liquid after quenching

Yen-Shuo Su, Chong-Wai Io, and Lin I

Department of Physics and Center for Complex Systems, National Central University, Zhongli, Taiwan 32001, Republic of China

(Received 20 February 2011; published 18 July 2012)

The spatiotemporal evolutions of microstructure and motion in the transient relaxation toward the steady supercooled liquid state after quenching a dusty plasma Wigner liquid, formed by charged dust particles suspended in a low pressure discharge, are experimentally investigated through direct optical microscopy. It is found that the quenched liquid slowly evolves to a colder state with more heterogeneities in structure and motion. Hopping particles and defects appear in the form of clusters with multiscale cluster size distributions. Via the structure rearrangement induced by the reduced thermal agitation from the cold thermal bath after quenching, the temporarily stored strain energy can be cascaded through the network to different newly distorted regions and dissipated after transferring to nonlinearly coupled motions with different scales. It leads to the observed self-similar multiscale slowing down relaxation with power law increases of structural order and structural relaxation time, the similar power law decreases of particle motions at different time scales, and the stronger and slower fluctuations with increasing waiting time toward the new steady state.

DOI: [10.1103/PhysRevE.86.016405](https://doi.org/10.1103/PhysRevE.86.016405)

PACS number(s): 52.27.Lw, 61.20.Lc

I. INTRODUCTION

As the liquid is cooled to the glass forming state, the dynamics becomes slow [1,2]. In the past decade, its microstructure and motion have attracted a great deal of attention, especially through numerical simulation and direct optical microscopy at the discrete level [3–12]. Systems with Lennard-Jones-type potentials [4,6,12], colloidal suspensions [3,9–11], granular systems [7], dusty plasma liquids [5,13–15], etc., are the few model systems. The structural and dynamical heterogeneities are the observed distinct generic features regardless of the different types of systems [1–12]. Namely, various sized crystalline-ordered domains (CODs) and the surrounding defect clusters coexist. Under the stochastic thermal kicks, particles exhibit stick-slip-type motion with alternate small amplitude rattling in the cage formed by the nearest neighbors and avalanche cooperative hopping over caging barriers after accumulating sufficient constructive perturbations. Avalanche cooperative hopping occurs in the form of clusters involving various numbers of particles and causes structural rearrangement [3,5,12]. With decreasing temperature, the increasing averaged size of immobile domains and the lower hopping rate cause the slower dynamics [3,5–7,10]. The studies for the slow microdynamics have been mainly conducted at different *steady states* [3–7,11,12]. The transient slowing-down relaxation process with increasing waiting time t_w from quenching to the colder glass forming liquid remains to be a poorly understood issue [8,10], especially in experimental studies of its spatiotemporal evolution and scaling behaviors.

Microscopically, the heterogeneous network with multiscale structure and motion is a consequence of the competition between the correlation from mutual interaction and the disorder from reduced stochastic thermal agitation. It prevents the homogeneous and independent local relaxation, and thereby the intuitive exponential slowing down after quenching. After quenching, in addition to quickly dissipate the kinetic energy, the colder thermal bath still provides thermal kicks to slowly release and transfer the stored strain energy to different regions and motions at different scales, through strong nonlinear coupling and induced structural

rearrangement. How microstructure and motion at different scales evolve, and their spatiotemporal scaling behaviors in the transient relaxation toward the new equilibrium liquid after quenching are interesting unexplored issues. In this work, those issues are experimentally investigated for the first time using a quenched quasi-two-dimensional (2D) dusty plasma liquid through directly tracking individual dust motion.

The dusty plasma liquid (DPL) can be formed by micrometer sized dusts suspended in the low pressure rf discharge [5,13–18], through the screened Coulomb interaction due to strong negative charging ($\sim 10^4$ e/dust) on dusts. Dust motion can be directly tracked through optical microscopy at the discrete level. It makes the dusty plasma liquid a platform to mimic and understand the generic microbehaviors of the Wigner liquid, complementarily to other model experimental systems with short range interaction, such as colloidal and granular systems [3,7,10,11]. Nevertheless, for the quenched DPL studies, only the structural order evolution to the *crystalline* state without correlating particle motions has been investigated by using the monolayer 2D DPL [16–18].

In this work, the quasi-2D DPL is quenched to the supercooled liquid by the sudden reduction of rf power. With increasing waiting time t_w from quenching toward the new steady state, how the structural and dynamical heterogeneities slowly evolve are investigated by correlating spatiotemporal evolutions and scaling behaviors of microstructure and motion. The following results are found: (a) The quenched liquid exhibits self-similar multiscale heterogeneities in structural and motion. The degree of heterogeneity increases with t_w . (b) The transient slowing down with decreasing mean square displacement MSD is associated with the two-stages power law increases and leveling off of the structural order, the averaged size of CODs, the structural relaxation time, and the fluctuation level. (c) MSD_τ at different time interval τ exhibit the self-similar power law decays with increasing t_w . A picture with the slow strain energy cascading through the network involving self-similar multiscale dynamics via thermal induced hopping and structural rearrangement is constructed to explain the above new findings.

II. EXPERIMENT

The experiment is conducted in a cylindrical symmetric rf dusty plasma system [Fig. 1(b)], similarly to what described elsewhere [5,19]. A hollow coaxial cylindrical trap with 4.1 (4.3) cm inner (outer) diameter, and 14 mm height is put on the bottom electrode, in which the DPL formed by polystyrene particles ($7 \pm 0.4 \mu\text{m}$ in diameter, with 10% standard deviation of particle diameter) are confined by the sheath field adjacent to the trap wall. The weakly ionized glow discharge ($n_e \sim 10^9 \text{ cm}^{-3}$) is generated in 250 mTorr Ar gas using a 14-MHz rf power system. The wake field effect of the downward ion wind toward the bottom electrode lines up dusts into vertical chains [20], with about 14 dusts in each chain. Figure 1(b) shows a snapshot of the side view images of the short chains of the supercooled liquid, illuminated by a thin vertical laser sheet.

The dust (chain) positions in the horizontal plane illuminated by an expanded thin horizontal laser sheet are digitally tracked by a CCD camera with 1024×768 pixels and operated at 30 Hz sampling rate. The total number of particles in an image frame N_{tot} is about 900. The mean interchain distance a , the mean vertical interparticle distance, and the dust mass are about 0.3 mm, 0.27 mm, and 1.9×10^{-10} g/dust, respectively. The sudden drop of the rf power from 2.3 to 1.6 watt in 1 ms causes the sudden drops of plasma density and the background thermal agitation, and the sudden change of the thickness of the surrounding sheath adjacent to the wall. The dusts are quickly realigned in the initial 1 s to form new vertical chains without vertical flipping. It makes us set $t_w = 0$ at 1.0 s after the sudden rf power drop. The background plasma has also reached the new steady state before $t_w = 0$. The estimated Debye length and the estimated charges on the dust are in the order 10^{-1} mm and from a few to ten thousands of electrons per dust. The frustrations of the microstructure due to the polydisperse dust size distribution (dust charges \propto dust diameter) in this quasi-2D system prevent direct crystallization after quenching. Ten runs with the same quenching processes are used to obtain the statistical information.

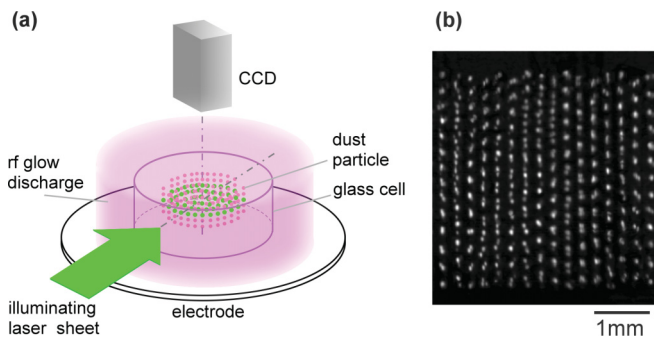


FIG. 1. (Color online) (a) The sketch of the experimental system. The dusts are confined by the center glass cell and suspended in the plasma above the bottom electrode. The motion of the dusts (green/dark gray dots) illuminated by the horizontal laser sheet are recorded by a CCD. (b) The snapshot showing the side view image of the short vertical chains illuminated by a thin vertical laser sheet. The thickness of the laser sheet is about one a . The dim dust images nearby the bright dust images along the same vertical chain are contributed by the particles along the adjacent vertical chain at different viewing depth.

The short vertical chains (14 particles in each chain) are stiff and stable. Particles along the same chain tend to move together horizontally without vertical flipping. Namely, the particle vertical positions along the chain cannot be rearranged. In the ordered horizontal domains, the straight chains remain vertical and exhibit only small amplitude wiggling due to horizontal cage rattling. When horizontal hopping occurs, particles along the same chain hop nearly together. If there are very slight phase shifts of horizontal hopping of particles at different heights along the same chain, the slightly tilted chain is quickly restraightened at the end of hopping through the strong vertical coupling. The breaking fraction of the vertical chains connecting adjacent horizontal layers is less than 0.1% in the time scale of horizontal structural relaxation. The chain wiggling, tilting, and breaking cause only less than 1% deviation on the horizontal structural orders of adjacent layers. Those numbers are factors of two to three lower than those from the previous study for the much hotter liquid with much longer and softer chains (40 dusts per chain) [21]. Namely, the chain dynamics plays a negligible role on the dynamics in the horizontal plane. Adjacent layers share the highly similar horizontal microstructures, motions, and structural rearrangements. It makes the system a good quasi-2D system to understand the generic behaviors of the microstructure and motion of the 2D Yukawa liquid. Our previous studies showed that the cold quasi-2D liquid with short stiff chains exhibit similar generic behaviors on the microstructure and motion to other 2D Yukawa liquid [15].

III. RESULTS AND DISCUSSION

A. Microstructure and motion at different t_w

The bond-orientational order $\Psi_6(\mathbf{r}_j)$ is used for measuring the local structural order: $\Psi_6(\mathbf{r}_j) = \frac{1}{N_j} \sum_k \exp(i6\theta_{jk})$, where θ_{jk} is the angle of the bond from particle j at \mathbf{r}_j to its nearest neighbor k , and N_j is the number of its nearest neighbors [22]. $|\Psi_6|$ decreases with increasing local strain. $|\Psi_6| = 1$ and < 0.4 for the perfect lattice site and the defect site with the nearest neighbor number deviating from six, respectively [5,22].

Figures 2(a)–2(d) show the typical snapshots of triangulated microstructures with $|\Psi_6|$ and 7 s particle trajectories starting at different t_w s. The structural and dynamical heterogeneities can be evidenced by the coexistence of the multiscaled CODs with large $|\Psi_6|$ and the multiscaled defect clusters around the interface of CODs to accommodate their different lattice orientations. Dusts have higher tendency to exhibit slow caged rattling in CODs and exhibit avalanche cooperative hopping in the region near defect clusters [5,13]. As t_w increases, the average size of CODs increases. The sequential snapshots of Fig. 2(e) show the typical structural evolution associated with the rotation, dissociation, and merging of CODs and the formation and annihilation of defects. In the latter stage after quenching (e.g., $t_w \geq 100$ s), avalanche cooperative hopping never stops. Through that, the microstructure still can be rearranged [see the different microstructures and motions of Figs. 2(c) and 2(d)]. Namely, quenching does not lead to the crystallization to solid. The growth of the averaged size of CODs is statistically evidenced by the increasing correlation length ξ_6 of the spatial correlation function $g_{6r} = \langle \Psi_6^*(0)\Psi_6(r) \rangle$

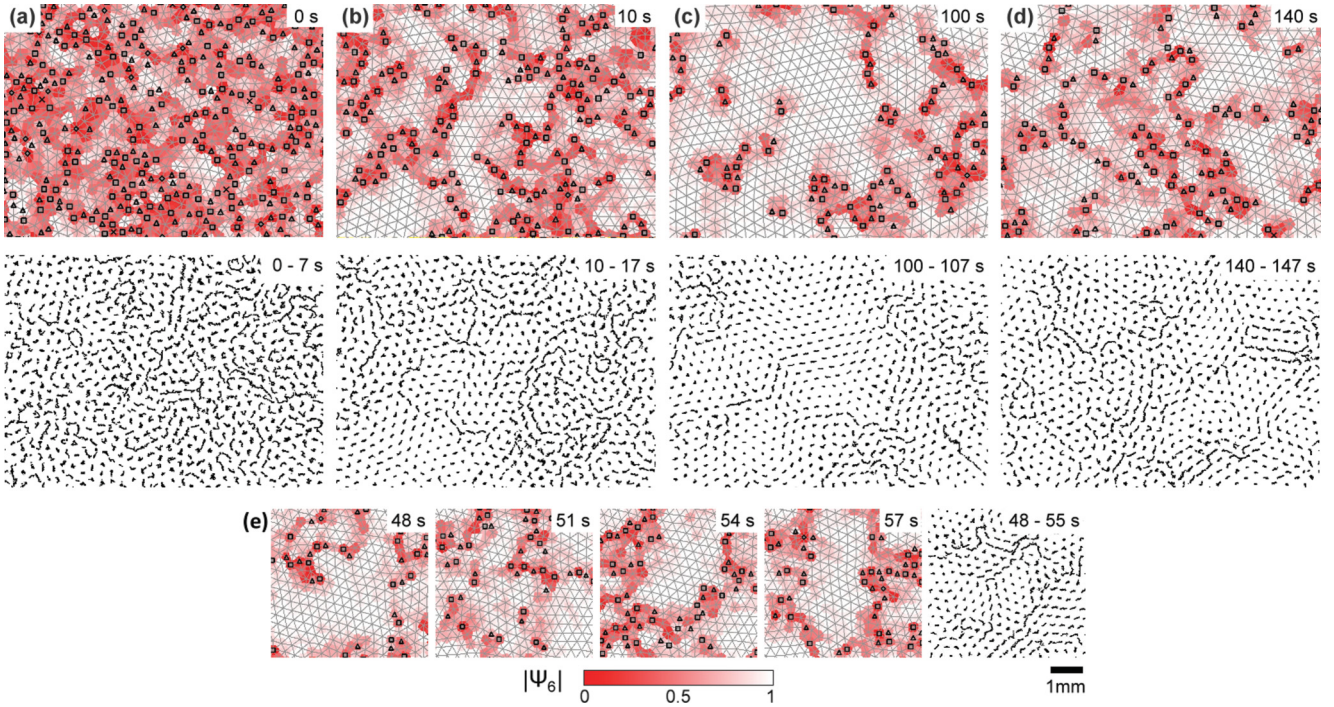


FIG. 2. (Color online) (a) to (d) The snapshots of microstructure (upper row) and 7 s particle trajectories (lower row) starting at different t_w . The background triangulated grids and the color indicate particle positions and the corresponding $|\Psi_6|$ for each exposure, respectively. The triangles and the squares correspond to the five- and the sevenfold defects, respectively. (e) The typical sequential snapshots of microstructure and the 7 s particle trajectories starting at $t_w = 48$ s, showing the structural order evolution through the dissociation and merging of CODs with the birth and annihilation of defects, and slight rotations of CODs.

with t_w , where ξ_6 is the length as g_{6r} reaches $1/e$ of its maximum [Fig. 3(a)].

Figure 3(b) shows the particle mean square displacement $\text{MSD}_\tau = \langle \Delta X_\tau^2 \rangle$ in time interval τ starting from a few different t_w ($t_w = 100$ s is time for reaching the new equilibrium state). $\langle \dots \rangle$ indicates the average over interval from t_w to $1.2 t_w$ (except over 1 s for $t_w = 0$) of ten repeated quenching runs for all the averaged quantities in this work. Similarly

to our previous findings of a cold steady state dusty plasma liquid [5], at small τ , the thermal-induced cage rattling causes the subdiffusion with the scaling exponent $\beta < 1$. Over larger τ , the accumulation of constructive thermal perturbation induces avalanche cooperative hopping, and consequently structural rearrangement (α relaxation). It causes the superdiffusion with $\beta > 1$ and the drop of the temporal correlation function of the structural order, $g_{6\tau}(t_w) = \langle \Psi_6^*(t_w) \Psi_6(t_w + \tau) \rangle$, as shown in Fig. 3(c). Note that the temporal correlation time τ_6 of $g_{6\tau}$ (the time as $g_{6\tau}$ reaches $1/e$ of its maximum), which corresponds to the averaged local structural relaxation time, is about the same order as the τ for the MSD reaching about $0.1 a^2$. With increasing t_w the increasing τ_6 , the increasing $g_{6\tau=0s} (= |\Psi_6|^2)$, and the rightward shift of the similar curves of MSD_τ evidence the slowing down with the better structural order, the slower structural rearrangement rate, and the slower self-similar anomalous diffusion.

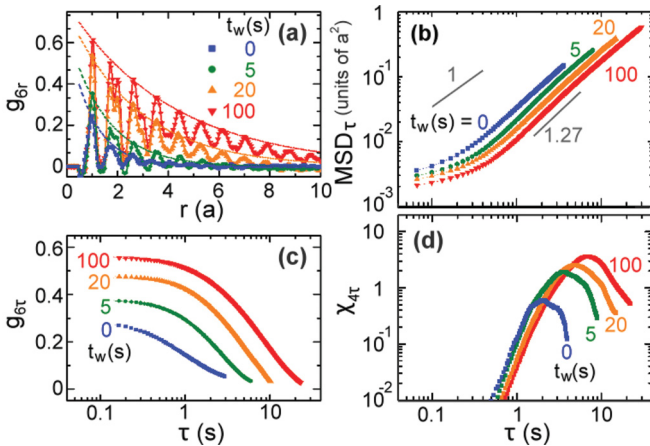


FIG. 3. (Color online) (a) g_{6r} vs r at different t_w . The smooth curves show the best exponential fit for measuring the correlation length ξ_6 . (b)–(d) MSD_τ , $g_{6\tau}$, and $\chi_{4\tau}$, vs τ at different t_w . The numbers beside the straight gray lines in (b) indicate the scaling exponents.

B. Multiscale dynamical and structural heterogeneities at different t_w

Similarly to other steady state supercooled liquid studies [4,7,8,11,12], the four-point susceptibility $\chi_{4\tau} = N_{\text{tot}}(\langle Q_\tau^2 \rangle - \langle Q_\tau \rangle^2)$ at different t_w are measured to characterize the fluctuation level of the stick-slip motion, i.e., the degree of the dynamical heterogeneity, after quenching [Fig. 3(d)]. The overlap parameter Q_τ indicates the fraction of particles remaining caged over interval τ . It is obtained by averaging the overlap function $W(\Delta x_\tau)$, defined as $W(\Delta x_\tau) = 1(0)$, if $\Delta x_\tau \leq (>) 0.3 a$, over $N_{\text{tot}} (=900)$ particles [4,7]. χ_4 reaches the

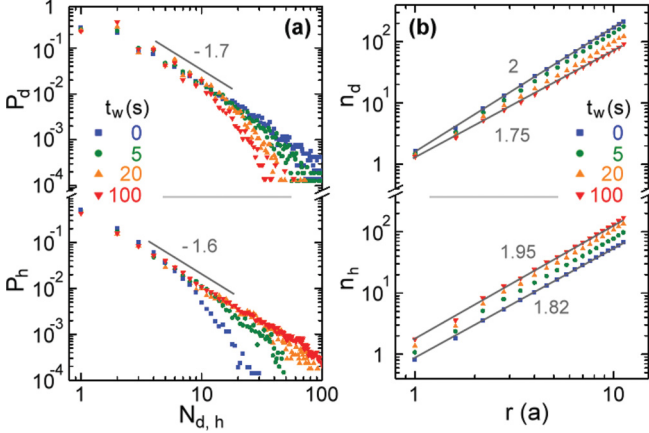


FIG. 4. (Color online) (a) The histograms P_d and P_h of the sizes of defect and hopping clusters in a 2D plane, respectively, at different t_w . (b) The averaged numbers of the defect sites (n_d) and the hopping sites (n_h) in circles centered at defect and hopping sites vs radius r . The scaling exponents indicated by the gray numbers are the correlation dimensions of the defects and hopping sites.

maximum value χ_4^* at τ^* , which is about the same order as the correlation time τ_6 (the time scale for avalanche cooperative hopping and structural rearrangement). The rightward and upward shifts of the similar curves of χ_4 in Fig. 3(d) manifest that the slowing down of dust motion and structural relaxation with the better structural order demonstrated in Figs. 3(b) and 3(c) is associated with the increasing dynamical heterogeneity with slower and stronger fluctuations. The behaviors are similar to the trends with decreasing temperature in other steady state glass-forming liquids [3–8,10–12], despite our softer interaction and the transient nature.

Similarly to the steady state three-dimensional (3D) supercooled colloidal liquid and the steady state cold quasi-2D DPL [3,5], our transient heterogeneous liquid after quenching still supports multiscale structure and cooperative motion. Defects and hopping particles both appear cooperatively in the form of clusters (Fig. 2), with various sizes N_d and N_h (numbers of particles in the 2D plane) for single clusters, respectively. Figure 4(a) shows that, at $t_w = 0$, the histogram $P_d(N_d)$ follows power law distribution with scaling exponent $= -1.7$ over a wide range of N_d . A faster descending tail appears as t_w increases. Defects also show the self-similar scale-free fractal spatial distribution [Fig. 4(b)]. The fractal (correlation) dimensions at different t_w s [23] are measured from the exponents of the double logarithmic plots of the averaged number of defects n_d in the circle centered at each defect with increasing radius r in the 2D plane [Fig. 4(b)]. It decreases from 2 to 1.75 as t_w increases from 0 to 100 s. These findings indicate that the defects appearing around the interfaces of CODs become more stringlike due to the growing COD size with t_w . It also suppresses the fat tail of the cluster size distribution.

On the other hand, the histogram $P_h(N_h)$ of cooperative hopping clusters (hopping dusts are defined as the dusts traveling more than $0.3a$ in τ^* for each t_w) exhibits an opposite trend to $P_d(N_d)$ with increasing t_w [Fig. 4(a)]. At $t_w = 100$ s, the power law scaling extends to the large N_h end with scaling exponent $= -1.6$. Avalanche cooperative hopping likes to

occur in the regions surrounding defect clusters and can also extend to the center region of the large COD for the dissociation of the COD [Fig. 2(b)]. With increasing t_w , the stronger spatial correlation under the better structural order tends to sustain larger width of avalanche cooperative hopping and change it from string- to band-like [Fig. 2(b)]. Its competition with thermal agitation makes the system more critical-like with the power law scaling of P_h extending to the larger N_h regime and increases the fractal distribution of hopping sites to more 2D like with n_h increasing from 1.82 to 1.95 [Fig. 4(b)]. The power law scaling indicates the similar dynamical selection rule over a wide range of scales for the cooperative hopping are obeyed. The extended tail in P_h causes the increased averaged N_h involved in structure rearrangement. It is reminiscent of the Adam and Gibbs hypothesis [24] and the recent experimental observation in the aging of the binary colloidal glass [10].

C. Temporal scaling behaviors of structural order and motion with increasing t_w

Now let us focus on the temporal scaling behaviors in the slowing down with increasing t_w , as depicted in Fig. 5. The structural order parameters such as defect fraction (f_D), $\langle |\Psi_6| \rangle$, ξ_6 , and τ_6 , averaged over ten quenching runs mainly follow the two-stage power law scaling and then level off after reaching new equilibrium at $t_w = 100$ s. The scaling exponents of both f_D and $1 - \langle |\Psi_6| \rangle$ equal -0.03 and -0.17 for the first and second stages, respectively. Our $t_w = 0$ was chosen right after the vertical chain realignment induced by the strong sheath variation associated with the rf power reduction. For $t_w < 2$ s, the time is too short to accumulate sufficient constructive perturbation for inducing sufficient avalanche cooperative hopping and structural rearrangements. Namely, most regions have small changes of their structural orders in this short time scale. It leads to the smaller scaling exponent

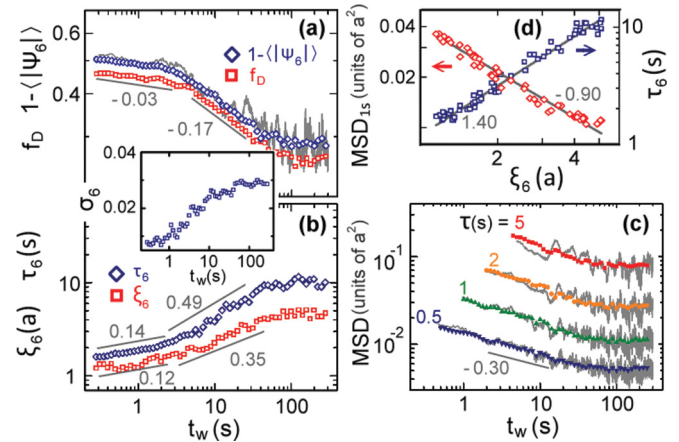


FIG. 5. (Color online) (a) to (c) The averaged defect fraction (f_D) and $1 - \langle |\Psi_6| \rangle$ (a), τ_6 and ξ_6 (b), and MSD_τ (c), vs t_w . The inset shows σ_6 versus t_w . The data of each curve at each t_w from (a) to (c) are obtained by averaging over the time interval from t_w to $1.2 t_w$ of 10 quenching runs, except the gray continuous curves with large fluctuations in (a) for $1 - \langle |\Psi_6| \rangle$ and in (c) for MSD_τ from a single quenching run without temporal and ensemble averages. (d) τ_6 and MSD_{1s} vs ξ_6 . The gray numbers nearby the straight lines from (a) to (d) indicate the scaling exponents.

of the first stage. The transition time scale is about the same time scale of τ_6 from the $g_{6\tau}$ curve of $t_w = 0$ s in Fig. 3(c). Note that, in the recent study of the monolayer dusty plasma liquid quenched to the final *crystalline* state, two-stage power law decay of defect fraction was also found [18]. In that study, the starting time $t_w = 0$ s was set right at the time for adjusting the rf power control parameter. The induced strong sheath variation causes the initial ballistic dust motion. It in turn causes faster structural rearrangement and the more negative scaling exponent for the drop of defect fraction than those in our system. Also note that, comparing their first stage and our second stage both end at $\xi_6 \sim 5a$, the ratio of the scaling exponent of ξ_6 to that of defect fraction are similar (~ -0.5).

The averaged MSD_τ s over ten quenching runs at different τ s show the similar power law decay (with scaling exponent = -0.30) toward the new equilibrium value with increasing t_w [Fig. 5(c)]. The gray curves with large fluctuations in Figs. 5(a) and 5(c) depict the curves of $1 - \langle |\Psi_6| \rangle$ versus t_w and MSD_τ s versus t_w for a single quenching run, respectively. The fluctuations become larger and slower with increasing t_w until saturation around $t_w = 100$ s. The inset of Fig. 5(a) shows how σ_6 , the variance of $\langle |\Psi_6| \rangle$ from 10 quenching runs, increases with t_w until saturation. The leveling-off of all the averaged variables for $t_w > 100$ s indicates that the system enters a new equilibrium state with the colder thermal bath. The remaining large fluctuations associated with the hopping and structure change shown by Figs. 2(c) and 2(d) manifest that the system never becomes a solid after the slow growth and saturation of averaged COD size.

From the view of energy landscape for glass aging, the gradual decrease of strain energy with the increasing averaged COD size in the relaxation makes the system better trapped in the deeper valley of the energy landscape (larger ξ_6) [1,2]. The weak agitation from the colder thermal bath after quenching needs a longer time to drive the system climbing over the larger barrier to other lower energy states with larger CODs via structural rearrangement. It slows down the dynamics. Beyond that, to our knowledge, there is no theory at the kinetic level for the behaviors of spatiotemporal microdynamical evolution and scaling for the quenching relaxation to the supercooled liquid.

D. Micropicture of the transient slowing down relaxation

We construct the following micropicture to understand our observations. Our dusty plasma liquid is suspended in the neutral Ar gas. The 100 s global relaxation time scale is much longer than the 10 ms damping time due to dust collision with the background neutral gas [25]. Namely, after quenching, the kinetic energy of the hot liquid is quickly dissipated to the colder thermal bath through dust neutral collisions in the order of 10 ms. However, the strain energy stored in the disordered regions (the strain energy increases monotonically with the decreasing $|\Psi_6|$) cannot be instantaneously released and dissipated to the neutral gas. It takes time for dusts to accumulate constructive perturbation from the colder thermal bath for surmounting the caging barriers and induce hopping and structural rearrangement. Through that, the temporarily locked strain energy before quenching can

be slowly released to excite different modes of dust motions through nonlinear strong mutual interaction. The energy can either be transferred to other newly distorted regions and restored as strain energy again, or dissipated to the neutral gas background. This energy cascade involves multiscale structure and motion. It is evidenced by the self-similar power scaling of MSD and χ_4 curves in Fig. 3, and the size and the spatial distributions of defect clusters and hopping clusters in Fig. 4.

The gradual strain energy release with t_w causes the slow reduction of the averaged fraction of defects and the slow growth of the averaged size of the ordered domains. It makes more particles better locked, which further slows down the dynamics and the domain growth rate. It provides a self-similar feedback for the transient slowing down relaxation dynamics, associated with the power law increases of τ_6 , ξ_6 , and $\langle |\Psi_6| \rangle$ with t_w , until reaching a new steady colder state. Figure 5(d) also show the faster increase of τ_6 than ξ_6 with increasing t_w ($\tau_6 \propto \xi_6^{1.4}$ and ξ_6 is proportional to the averaged scale of the COD). The self-similar power law scaling of MSD_τ [Fig. 5(c)] for different τ with increasing t_w is a consequence of the above multiscale energy transfer process through the nonlinearly coupled heterogeneous network. Note that MSD_τ/τ is the diffusivity reflecting the intensity of motion excitation at time scale τ . Our findings imply that the similar dynamical selection rules for energy cascading over modes with different scales are followed in the evolution toward new equilibrium. Correlating the data from Figs. 5(a) to 5(c) further reveals the following power law relations: $\text{MSD} \propto \xi_6^{-0.90}$.

What is the reason for the stronger and the slower fluctuation in the slowing down process? Microscopically, with increasing t_w , CODs cannot monotonically grow due to the different lattice orientations of the adjacent CODs. The long time growth of averaged COD size is accompanied with the rotation, dissociation, and merging of CODs and reorganizing of defect clusters. It involves multiscale avalanche cooperative hopping as shown in the examples of Fig. 2(e). The more extended tail of the histogram of the hopping cluster size with increasing t_w in Fig. 4(a) implies that, as averaged COD size growth, the structural rearrangement involves a larger number of cooperatively moving particles. It also causes the slower and larger fluctuation, as manifested by the inset of Fig. 5(a) and the gray continuous single-run curves of $\langle |\Psi_6| \rangle$ and MSD_τ s in Figs. 5(a) and 5(c), respectively. The findings also agree with the behavior of the larger and slower fluctuation associated with χ_4 as t_w increases to 100 s, shown in Fig. 3(d). The different microstructure and motion between Figs. 2(c) and 2(d) further illustrate the large fluctuation through avalanche cooperative hopping after the averaged structural order levels off after $t_w = 100$ s.

From the more general view of nonlinear complex systems, the stick-slip-type avalanche excitation by thermal agitation under the effect of the strong nonlinear coupling with neighboring particles makes the steady state cold or supercooled liquid belong to the general category of the nonlinear coupled subexcitable many body systems driven by noise [5,26,27]. The thermal agitation provides energy to excite and de-excite motion. The strong coupling on one hand sets up topological constraint and thereby the caging threshold for hopping. On the other hand, the strong coupling is also a channel to transfer and

dissipate the energy of the hopping particle to the neighboring particles. It can induce avalanche cooperative hopping, or stop avalanche cooperative hopping if the neighboring particles are in the states far from the caging threshold. This makes hopping excitation subexcitable in the stick-slip form. This type of nonlinear coupled subexcitable many body systems under stochastic or slow drives exhibits generic SOC (self-organized criticality) behaviors, i.e., critical-like self-similar spatiotemporal power law scaling behaviors for the multiscale avalanche-type excitations over a wide range of the control parameter [5,13,26,27]. Our study sheds light on understanding the rarely studied generic transient dynamical behaviors of the microscopic SOC systems after quenching to a state under lower stochastic driving.

IV. CONCLUSION

In conclusion, we have investigated the transient relaxation dynamics of a supercooled Wigner DPL. The interplay of mutual interaction and reduced thermal agitation after quenching is the key to generate the observed nonlinear heterogeneous network exhibiting multiscaled microstructure and motion. It in turn supports the multiscale slowing down dynamics with structural rearrangement, through the alternate cage rattling and avalanche cooperative hopping. After quenching, the kinetic energy is quickly dissipated to the colder thermal bath

in the order of 10 ms. Nevertheless, the strain energy stored in the heterogeneous network before quenching cannot be instantaneously released. Through the stick-slip cooperative avalanche hopping, the strain energy can be cascaded through the network to different newly distorted regions and dissipated to the background thermal bath after transferring to nonlinearly coupled motions with different scales. It slowly increases the averaged size of CODs, in which the better particle interlocking further slows down motion and structural rearrangement, and causes larger fluctuation, associated with the merging and the dissociation of CODs involving larger averaged N_h in structural rearrangement. The observed two-stage power law temporal scaling of increasing structural order, the similar temporal power law scaling of decreasing MSD_τ for different τ , the power law relations among τ_6 , ξ_6 , MSD_τ , and $\langle |\Psi_6| \rangle$; and the power law scaling of defects and avalanche cooperative hopping cluster sizes evidence the self-similar slowing down dynamics over different spatiotemporal scales of this SOC-like system.

ACKNOWLEDGMENT

This work is supported by the National Science Council of the Republic of China, under contract No. NSC99-2112-M008-002-MY3.

-
- [1] M. D. Ediger, C. A. Angell, and S. R. Nagel, *J. Chem. Phys.* **100**, 13200 (1996).
 - [2] P. G. Debenedetti and F. H. Stillinger, *Nature (London)* **410**, 259 (2001).
 - [3] E. R. Weeks, J. C. Crocker, A. C. Levitt, A. Schofield, and D. A. Weitz, *Science* **287**, 627 (2000).
 - [4] S. C. Glotzer, V. N. Novikov, and T. B. Schröder, *J. Chem. Phys.* **112**, 509 (2000).
 - [5] Y. J. Lai and L. I, *Phys. Rev. Lett.* **89**, 155002 (2002).
 - [6] T. Kawasaki, T. Araki, and H. Tanaka, *Phys. Rev. Lett.* **99**, 215701 (2007).
 - [7] K. Watanabe and H. Tanaka, *Phys. Rev. Lett.* **100**, 158002 (2008).
 - [8] A. Parsaeian and H. E. Castillo, *Phys. Rev. Lett.* **102**, 055704 (2009).
 - [9] L. Assoud, F. Ebert, P. Keim, R. Messina, G. Maret, and H. Lowen, *Phys. Rev. Lett.* **102**, 238301 (2009).
 - [10] P. Yunker, Z. Zhang, K. B. Aptowicz, and A. G. Yodh, *Phys. Rev. Lett.* **103**, 115701 (2009).
 - [11] P. Yunker, Z. Zhang, and A. G. Yodh, *Phys. Rev. Lett.* **104**, 015701 (2010).
 - [12] R. Candelier, A. Widmer-Cooper, J. K. Kummerfeld, O. Dauchot, G. Biroli, P. Harrowell, and D. R. Reichman, *Phys. Rev. Lett.* **105**, 135702 (2010).
 - [13] Y. H. Huang and L. I, *Phys. Rev. E* **76**, 016403 (2007).
 - [14] B. Liu, J. Goree, and O. S. Vaulina, *Phys. Rev. Lett.* **96**, 015005 (2006).
 - [15] C. L. Chan, C. W. Io, and L. I, *Contrib. Plasma Phys.* **49**, 215 (2009), and references therein.
 - [16] C. A. Knapek, D. Samsonov, S. Zhdanov, U. Konopka, and G. E. Morfill, *Phys. Rev. Lett.* **98**, 015004 (2007).
 - [17] Y. Feng, J. Goree, and B. Liu, *Phys. Rev. Lett.* **100**, 205007 (2008).
 - [18] P. Hartmann, A. Douglass, J. C. Reyes, L. S. Matthews, T. W. Hyde, A. Kovacs, and Z. Donko, *Phys. Rev. Lett.* **105**, 115004 (2010).
 - [19] L. W. Teng, M. C. Chang, Y. P. Tseng, and L. I, *Phys. Rev. Lett.* **103**, 245005 (2009).
 - [20] M. Nambu, S. V. Vladimirov, and P. K. Shukla, *Phys. Lett. A* **203**, 40 (1995).
 - [21] C. W. Io, C. L. Chang, and L. I, *Phys. Plasmas* **17**, 053703 (2010).
 - [22] K. J. Strandburg, *Bond-Orientational Order in Condensed Matter Systems* (Springer, New York, 1992).
 - [23] S. H. Strogatz, *Nonlinear Dynamics and Chaos* (Addison-Wesley, Reading, MA, 1994).
 - [24] G. Adam and J. H. Gibbs, *J. Chem. Phys.* **43**, 139 (1965).
 - [25] M. C. Chang, Y. P. Tseng, and L. I, *Phys. Plasmas* **18**, 033704 (2011).
 - [26] K. Rypdal, B. Kozelov, S. Ratynskaia, B. Klumov, C. Knapek, and M. Rypdal, *New J. Phys.* **10**, 093018 (2008).
 - [27] For example, P. Bak, C. Tang, and K. Wiesenfeld, *Phys. Rev. Lett.* **59**, 381 (1987); H. J. Jensen, *Self-Organized Criticality* (Cambridge University Press, Cambridge, 1998); J. Wang, S. Kádár, P. Jung, and K. Showalter, *Phys. Rev. Lett.* **82**, 855 (1999).